Generation of a temporally well-resolved sequence of snapshots of the flow-field in turbulent plane channel flow

Markus Uhlmann

Potsdam Institut für Klimafolgenforschung, D-14412 Potsdam
uhlmann@pik-potsdam.de

(July-Octobre 2000)

1. Purpose

In the framework of the research project of Klein (1998), detailed time-dependent information of the flow fields in two distinct geometric configurations (homogeneous, isotropic flow; plane channel flow) is needed for the purpose of analyzing the behavior of small-scale instabilities and their influence upon the turbulent energy cascade. Here we describe the current state of our ongoing effort of generating those fields via direct numerical simulation (DNS) in the latter case of plane channel flow.

2. The plane channel flow configuration and its simulation

In order to simulate flow in a plane channel, we solve the Navier-Stokes equations for an incompressible fluid in a box that is doubly periodic in the streamwise (x) and spanwise (z) directions and spans the full channel height $2h$ in the wall-normal direction (y; cf. figure 1).

Our numerical method is similar to that of Kim, Moin & Moser (1987) inasmuch as the governing equations are written in terms of the wall-normal vorticity ω_y and the Laplacian of the wall-normal velocity, $\varphi = \nabla^2 v$ (thereby eliminating all pressure terms). The spatial discretization is fully spectral, using Fourier series in (x, z) and a Chebychev polynomial expansion in y. The time discretization is third order Runge-Kutta for the non-linear convective terms - which are constructed in physical space using de-aliasing in (x, z) according to the 2/3 rule - and implicit Euler for the viscous terms. Note that no de-aliasing of Chebychev modes is employed in accordance with results of Uhlmann (2000*b*).

The velocity components are deduced from the evolution variables by means of the continuity equation and the definition of vorticity. The $(0, 0)$-mode of velocity (i.e. the (x, z)-planewise mean), however, is obtained directly by integrating the momentum equation in "primitive" variables, using a driving force that is equal to the global wall-friction. The mass flow-rate is explicitly kept constant (cf. details in appendix A) and the mean pressure gradient as well as the wall-shear stress are a function of time. Details of the numerical method and its implementation for multi-processor distributed memory machines can be found in Klein & Uhlmann (2000).

3. Scales in wall-bounded turbulent flows

In pipe or channel flow an integral balance of the ensemble-averaged momentum equation shows that the total shear stress varies linearly with wall-distance, with the wall shear

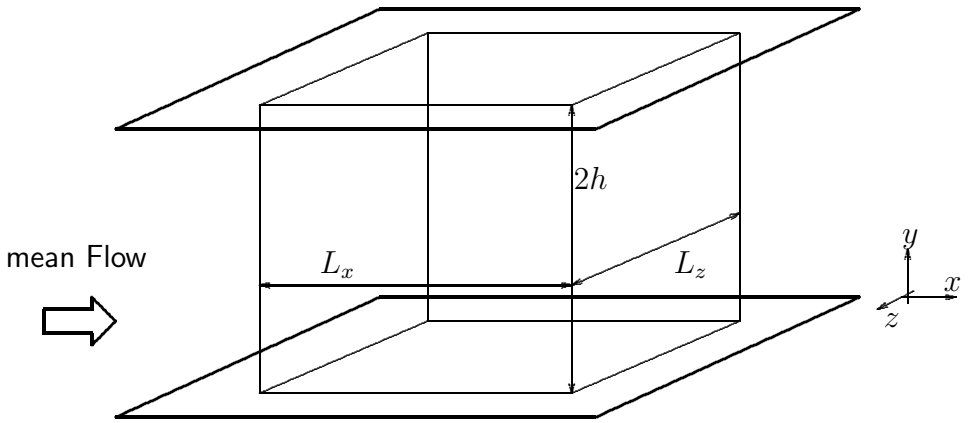

FIGURE 1. Schematic of the plane channel flow configuration and the rectangular computational domain of dimension $L_x \times 2h \times L_z$ in the streamwise, wall-normal and spanwise direction respectively.

stress $\pm\tau_w$ as the boundary condition on both sides. The friction velocity $u_\tau = \sqrt{\tau_w}$ can therefore be understood as a scale for the velocity fluctuations throughout the channel height. In the immediate vicinity of the wall, where turbulent fluctuations can be neglected with respect to viscous terms, mean velocity itself varies linearly with wall-distance which in turn leads to the definition of a viscous length scale $\delta_\tau = \nu/u_\tau$. So-called "wall-units" can then be defined and indicated by a "+"-superscript, e.g. dimensionless length $x^+ = xu_\tau/\nu$, velocity $v^+ = v/u_\tau$, time $t^+ = tu_\tau^2/\nu$ and vorticity $\omega^+ = \omega\nu/u_\tau^2$. At the wall, the viscous length scale is equivalent to the Kolmogoroff scale in isotropic turbulence $\delta_\tau \approx \eta$ (Jiménez 2000*b*). On the other hand, the friction Reynolds number $Re_\tau = u_\tau h/\nu$ takes the corresponding place of the large (integral) scale Reynolds number $Re_L = u'L/\nu$. The difference with idealized isotropic turbulence is that the two scales δ_τ and h are *spatially separated* (Jiménez 2000*b*):

> *We can think of the core of the pipe as 'normal' turbulence, with a full cascade and a full range of length scales. As we approach the wall, however, the large scales don't 'fit' anymore, and only the Kolmogorov range is left.*

In the zone of overlap between the two aforementioned regions, classical arguments lead to a logarithmic velocity profile. Let us simply mention that there exists an ongoing controversy in the literature concerning both, the adequacy of the use of the viscous velocity scale in the outer layer as well as the non-use of the outer length scale in the overlap region.

4. Some words on turbulence regeneration and autonomy

Jiménez & Moin (1991) identified what has become known as the "minimal flow unit" which is necessary for turbulence to be sustained in plane channel flow. Its extent scales in wall units and is given as $L_z^+ \approx 100$ and $L_x^+ \approx 250{-}350$. By reducing the periodic box to this elementary size, one effectively singles out an arrangement of an identical set of near-wall (i.e. buffer-layer) structures consisting of a pair of streaks and quasi-streamwise vortices.

More recently, Jiménez & Pinelli (1999) have shown the near-wall zone to be effectively autonomous, i.e. being capable to sustain "realistic" turbulence without any influence of the outer flow other than the existence of a mean shear. When all turbulent fluctuations

case	Re_τ	Re_0	Re_b	L_x	L_z	$N_x \times N_y \times N_z$	Δ_x^+	Δ_z^+	Δ_y^+
I	180	3250	2925	$3\pi h$	πh	$192\times 97\times 128$	8.8	4.4	5.9
II	395	7881	6876	$2\pi h$	πh	$256\times 193\times 256$	10.0	6.5	6.5
III	590	12486	10972	$2\pi h$	πh	$384\times 257\times 384$	9.7	4.8	7.2
IV	590	12486	10972	$2\pi h$	πh	$600\times 385\times 600$	6.1	3.0	4.8
V	190	3300	2970	$2\pi h$	πh	$600\times 385\times 600$	2.0	1.1	1.6

TABLE 1. Parameters of the different plane channel flow simulations: friction-velocity-based, centerline-velocity-based and bulk-velocity-based Reynolds number; box size; number of modes (before de-aliasing); equivalent grid size (note that Δ_y^+ corresponds to the maximum vertical grid size near the centerline) while the wall-normal Gauss-Lobatto grid point positions are given by $y_j^+ = (1 - \cos(\pi j/(N_y - 1)))\, Re_\tau$.

are explicitly filtered out above a height y_f in an artificial numerical experiment, the near-wall statistics remain relatively unchanged. The minimum filter height was determined as $y_f^+ \approx 70$.

The above mentioned minimal dimensions should be kept in mind when evaluating the dimensions of a given numerical simulation.

Of further concern is the size of quasi-streamwise correlated large structures in the logarithmic region of channel flow. With the continuous increase in feasible Reynolds numbers for numerical simulation and more recent careful experimental measurements, it becomes increasingly evident that a kind of "log-layer streak" needs to be considered as a characteristic structure, having an extent of approximately $L_x/h \approx 20$ and $L_z/h \approx 2$ (Jiménez 1998, 2000*a*; Miyake, Tsujimoto, Sato & Suzuki 2000). The requirements for simulating such large structures are beyond our present capabilities. On the other hand, the significance of those very large structures for the hypothesis of our present research project is most probably negligible.

5. Present series of simulations

Table 1 shows the parameters of the four present series of simulations. The three different Reynolds numbers and box sizes – except for case V which has a slightly smaller box than case I – are as in Moser, Kim & Mansour (1999) (AGARD Advisory Report No. 345 1997, cf. also). The first three cases also coincide with those references in terms of the grid resolution; case IV is a refinement of the high Reynolds number case and case V is a super-refined case with modest Reynolds number.

Equilibrium states for cases I to III have been obtained by the interpolation and temporal relaxation procedure described in Uhlmann (2000*a*). The previous reference also documents the quality of the statistics of cases II and III *before* starting to store individual snapshots. Due to constraints on the computational ressources, the most intensive cases IV and V are not run until statistics are fully converged after the initial transient is discarded (cf. figure 2 for the evolution of skin friction; figures 3-8 for the available statistics of limited quality).

Table 2 sums up the data production during the simulation series. Note that no snapshots have been generated for cases I, II so far since execution is possible on the local IBM SP2 machine and does not require a large computational effort.

Concerning the temporal increment between successive instantaneous fields, we decided to store after every elapsed wall-time unit, i.e. $\Delta t^+ = 1$, which happens to correspond to

	transient	statistics	no. of snapshots written
I	√	√	0
II	√	√	0
III	√	√	249
IV	√	–	240
V	√	–	250

TABLE 2. Details of the data generation for the different plane channel flow cases described in table 1.

10−11 (17) computational steps in case III (IV respectively) when a CFL-number of 0.5 is used.

The size of the *raw* data files (i.e. binary format 64bit floats, writing only the "useful" modes in Fourier space and restricting to the two variables ω_y and φ) is roughly 300MB and 1GB for cases III and IV/V respectively.

6. Proposed future series

Here we propose additional experiments which could be carried out in case that computational ressources are still available at the end of the present series.

Using the number of modes of cases IV or V, a case with an enlarged box could be run so that potentially more "events" would be present in one field.

During the course of the investigation it might turn out that a reduced box dimension is sufficient for our purpose so that even larger Reynolds numbers become accessible (or equally: even more extreme super-resolutions).

7. Acknowledgements

The code for the present simulation was kindly provided by J. Jiménez and A. Pinelli of ETSI Aeronauticos, Universidad Politécnica, Madrid. The computational resources of ZIB, Berlin, are gratefully acknowledged.

REFERENCES

AGARD Advisory Report No. 345 1997 A selection of test cases for the validation of large-eddy simulations of turbulent flows. available at ftp://138.4.75.138/.

JIMÉNEZ, J. 1998 The largest scales of turbulent wall flows. *CTR Res. Briefs* pp. 137–154.

JIMÉNEZ, J. 2000*a* Some open computational problems in wall-bounded turbulence. In *Advances in Turbulence VIII* (ed. C. D. et al.), pp. 637–646. Barcelona, Spain.

JIMÉNEZ, J. 2000*b* Turbulence. In *Developments in Fluid Mechanics: A Collection for the Milennium*. Cambridge U. Press (to appear).

JIMÉNEZ, J. & MOIN, P. 1991 The minimal flow unit in near-wall turbulence. *J. Fluid Mech.* **225**, 213–240.

JIMÉNEZ, J. & PINELLI, A. 1999 The autonomous cycle of near-wall turbulence. *J. Fluid Mech.* **389**, 335–359.

KIM, J., MOIN, P. & MOSER, R. 1987 Turbulence statistics in a fully developed channel flow at low Reynolds number. *J. Fluid Mech.* **177**, 133–166.

KLEIN, R. 1998 Kleinskalige Instabilitäten als Bausteine der turbulenten Energiekaskade. DFG-Antrag auf Gewährung einer Sachbeihilfe, Projekt KL 611/10 (in German).

KLEIN, R. & UHLMANN, M. 2000 Projektbeschreibung zum Großprojektantrag für den Paral-

lelrechner T3E des ZIB (in German). available under `www.pik-potsdam.de/~uhlmann/-projects.html`.

Miyake, Y., Tsujimoto, K., Sato, N. & Suzuki, Y. 2000 Structure of turbulence in the logarithmic layer and its mechanism. In *Advances in Turbulence VIII* (ed. C. D. et al.), pp. 403–406. Barcelona, Spain.

Moser, R., Kim, J. & Mansour, N. 1999 Direct numerical simulation of turbulent channel flow up to $Re_\tau = 590$. *Phys. Fluids* **11** (4), 943–945.

Uhlmann, M. 2000*a* Generation of initial fields for channel flow investigation. Intermediate Report, available under `www.pik-potsdam.de/~uhlmann/projects.html`, Potsdam Institute for Climate Impact Research, Potsdam, Germany.

Uhlmann, M. 2000*b* The need for de-aliasing in a Chebyshev pseudo-spectral method. Technical Note No. 60, available under `www.pik-potsdam.de/~uhlmann/projects.html`, Potsdam Institute for Climate Impact Research, Potsdam, Germany.

Appendix A. Constant mass flow-rate condition

The present condition for ensuring a constant mass flow-rate in pressure-driven plane channel flow has been suggested by A. Pinelli (personal communication). We consider the discrete equation for the constant-mode velocity U_{00} at a given Runge-Kutta sub-step:

$$U_{00}'' - \beta^2\, U_{00} = RHS + A \quad , \tag{A 1}$$

where $\beta = Re/\Delta t$, Re the Reynolds number, Δt the current time step, superscript $''$ denoting differentiation with respect to the spatial coordinate y, RHS includes the non-linear terms and A is the driving (pressure-gradient) term to be determined under the condition of constant mass flow-rate $Q_0 = \int_0^2 U_{00}\mathrm{d}y/2$. We split the linear problem into two parts: $U_{00} = u_1 + u_2$, where u_1 is the (numerically obtained) solution of the problem (A 1) with $A = 0$ and u_2 satisfies the counterpart $u_2'' - \beta^2\, u_2 = A$; both sub-problems are subject to the no-slip boundary condition $u_i(0) = u_i(2) = 0$. The latter problem admits the following analytical solution:

$$u_2 = A\,\frac{\Delta t}{Re}\,\frac{e^{\beta y} + e^{-\beta(y-2)} - 1 - e^{2\beta}}{1 + e^{2\beta}} \quad , \tag{A 2}$$

whith the associated flow-rate

$$Q(u_2) = -A\,\frac{\Delta t}{Re}\,\underbrace{\frac{\beta\, e^{2\beta} + \beta + 1 - e^{2\beta}}{\beta\,(1 + e^{2\beta})}}_{\equiv\, h(\beta)} \quad . \tag{A 3}$$

The forcing term is then simply obtained from the condition that $Q(u_1) + Q(u_2) = Q_0$, viz.

$$A = \frac{Re}{\Delta t\, h(\beta)}\,(Q(u_1) - Q_0) \quad . \tag{A 4}$$

Note that $\lim_{\beta\to\infty} h(\beta) = 1$ which is a very good approximation for practical values of β which almost always exceed $\mathcal{O}(10^5)$.

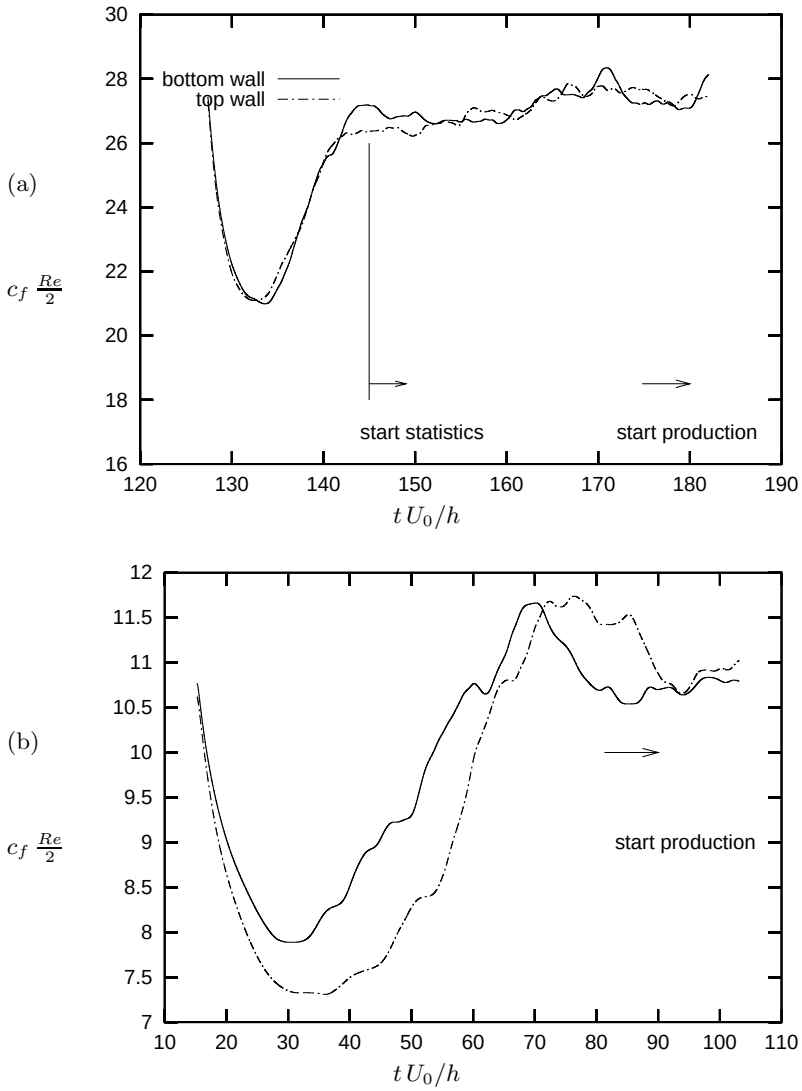

FIGURE 2. Temporal evolution of the plane-averaged skin friction c_f during the initial sequence of the plane channel flow simulations: (a) case IV ($Re_\tau = 590$); (b) case V ($Re_\tau = 190$). The initial transient is due to the generation procedure of the initial field. The two lines correspond to values averaged over the top and bottom wall-plane respectively.

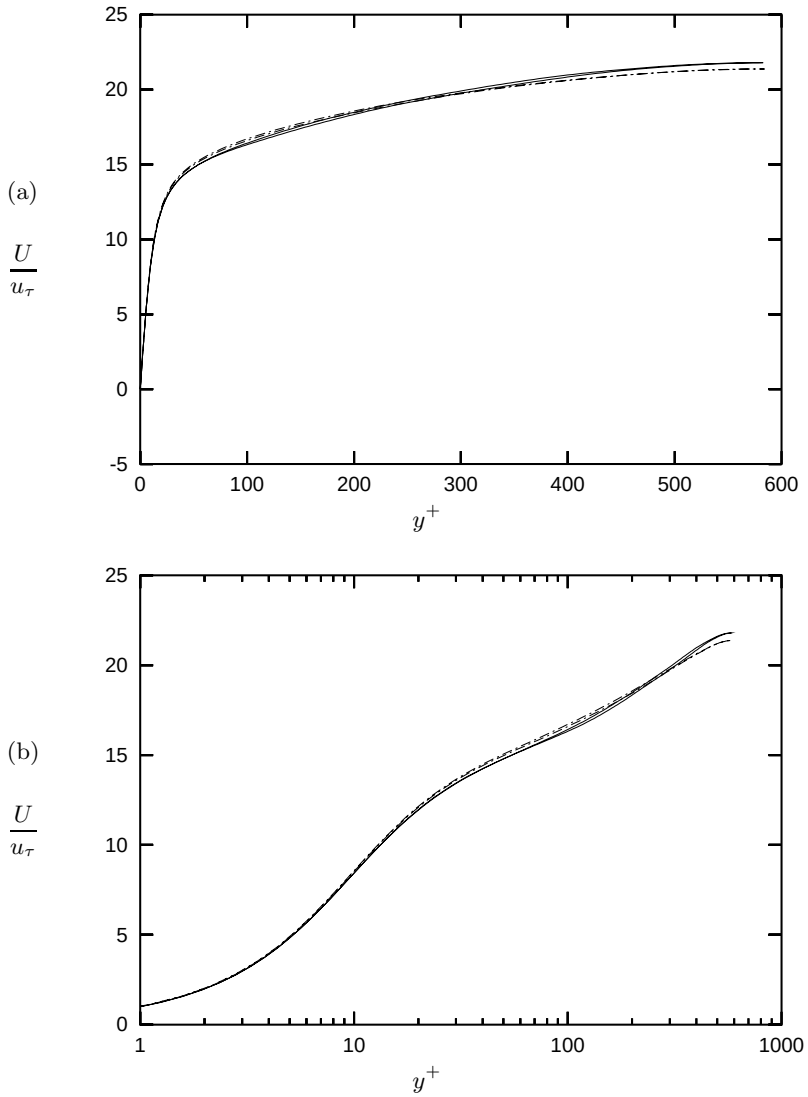

FIGURE 3. Mean velocity profile of the $Re_\tau = 590$ case: ——— , run IV; —·— , Moser *et al.* (1999). Lines for the bottom and the top half of the channel are superposed such as to provide an estimate of the statistical uncertainty. (a) lin-lin plot; (b) log-lin plot.

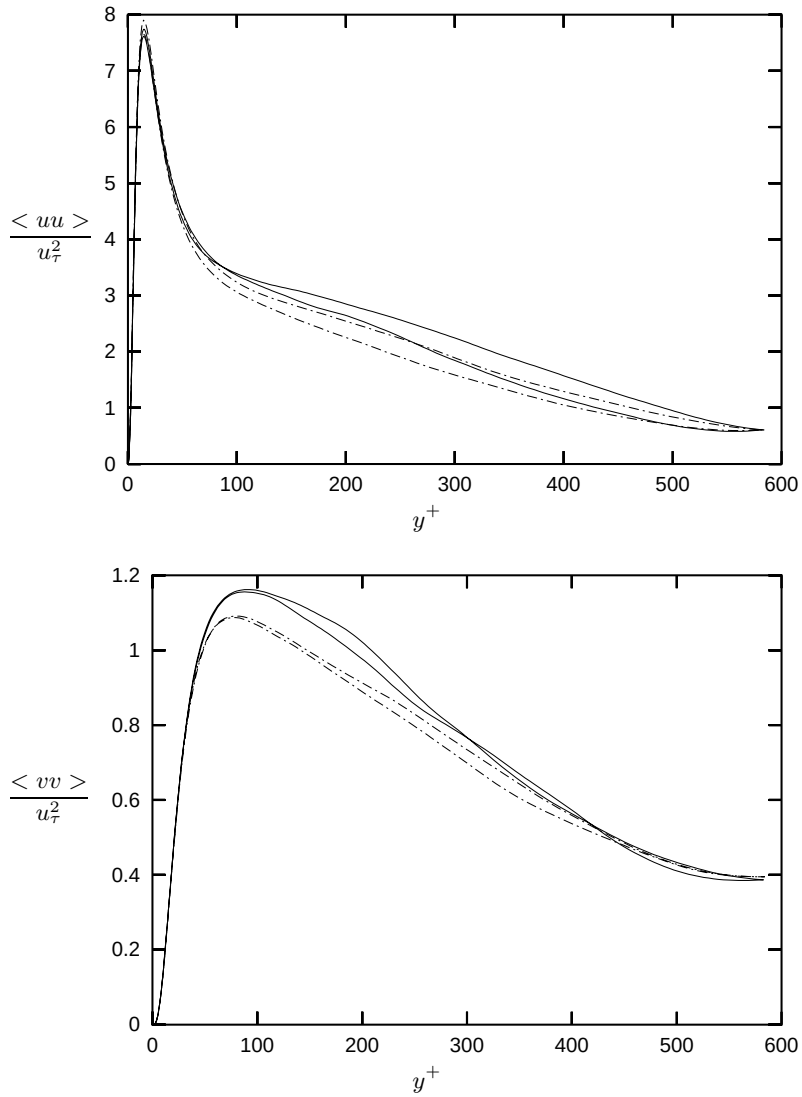

FIGURE 4. Wall-normal profile of various components of the Reynolds stress tensor of the $Re_\tau = 590$ case. Legend as in figure 3.

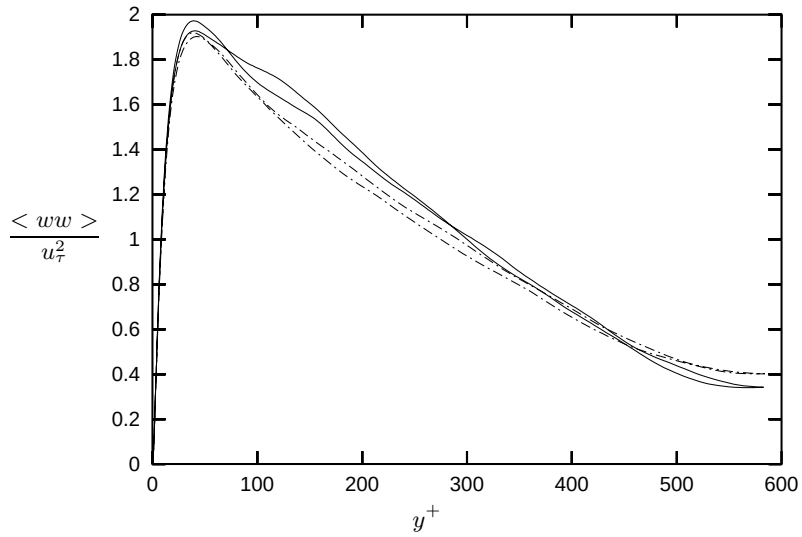

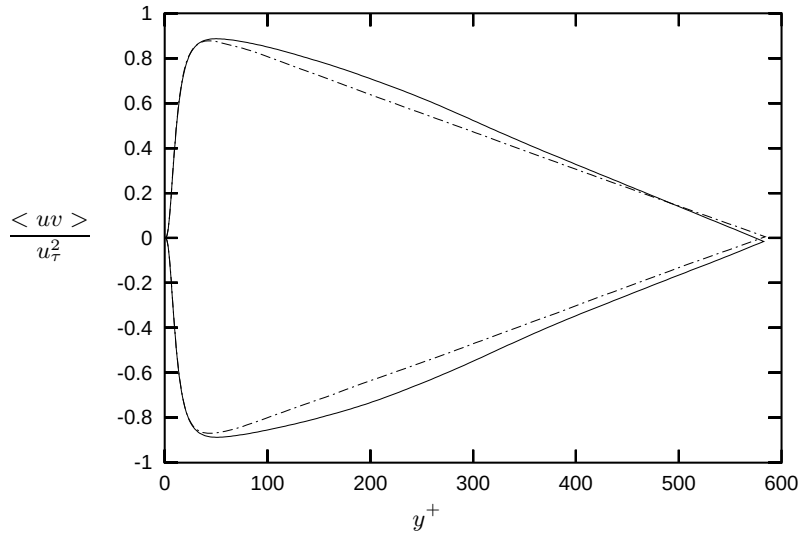

FIGURE 4. *(continued)*

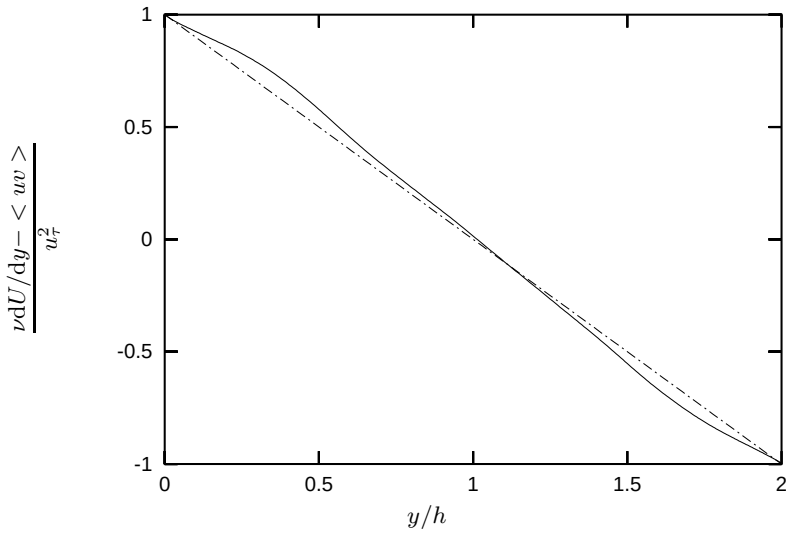

FIGURE 5. Wall-normal profile of the total shear stress of the $Re_\tau = 590$ case. Legend as in figure 3.

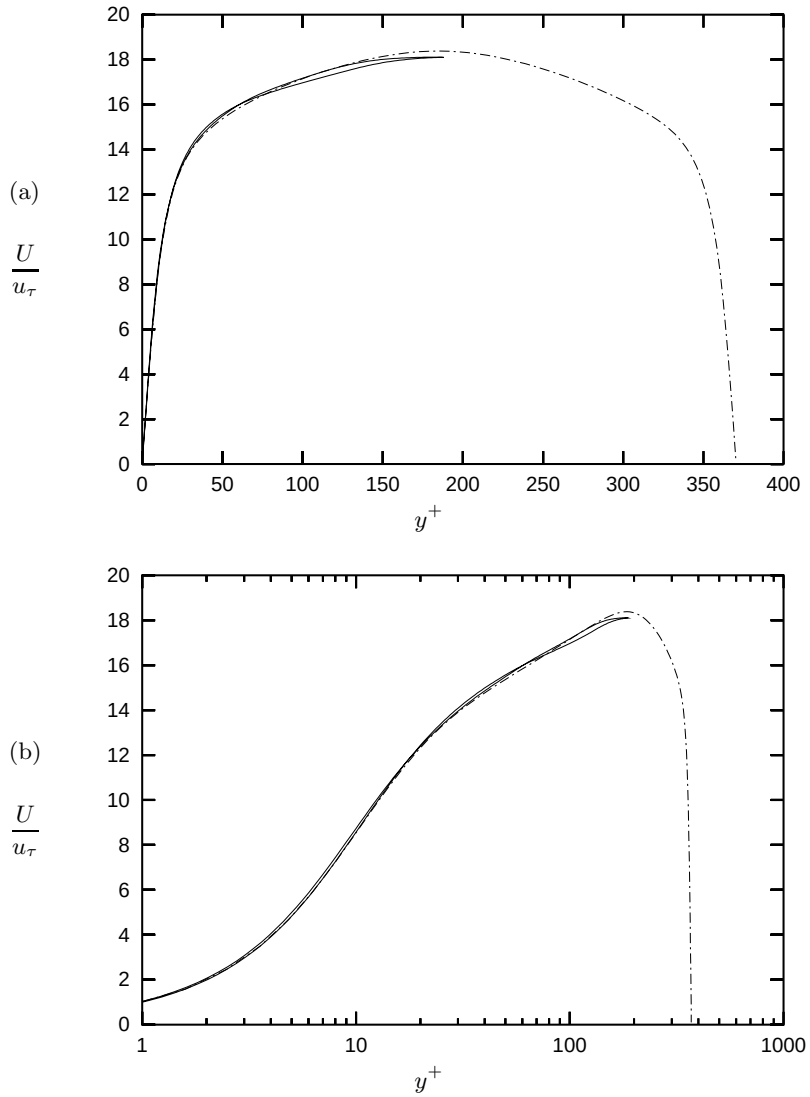

FIGURE 6. Mean velocity profile of the $Re_\tau = 190$ case: ——— , run V; —·— , Kim *et al.* (1987). Lines for the bottom and the top half of the channel are superposed such as to provide an estimate of the statistical uncertainty. (a) lin-lin plot; (b) log-lin plot.

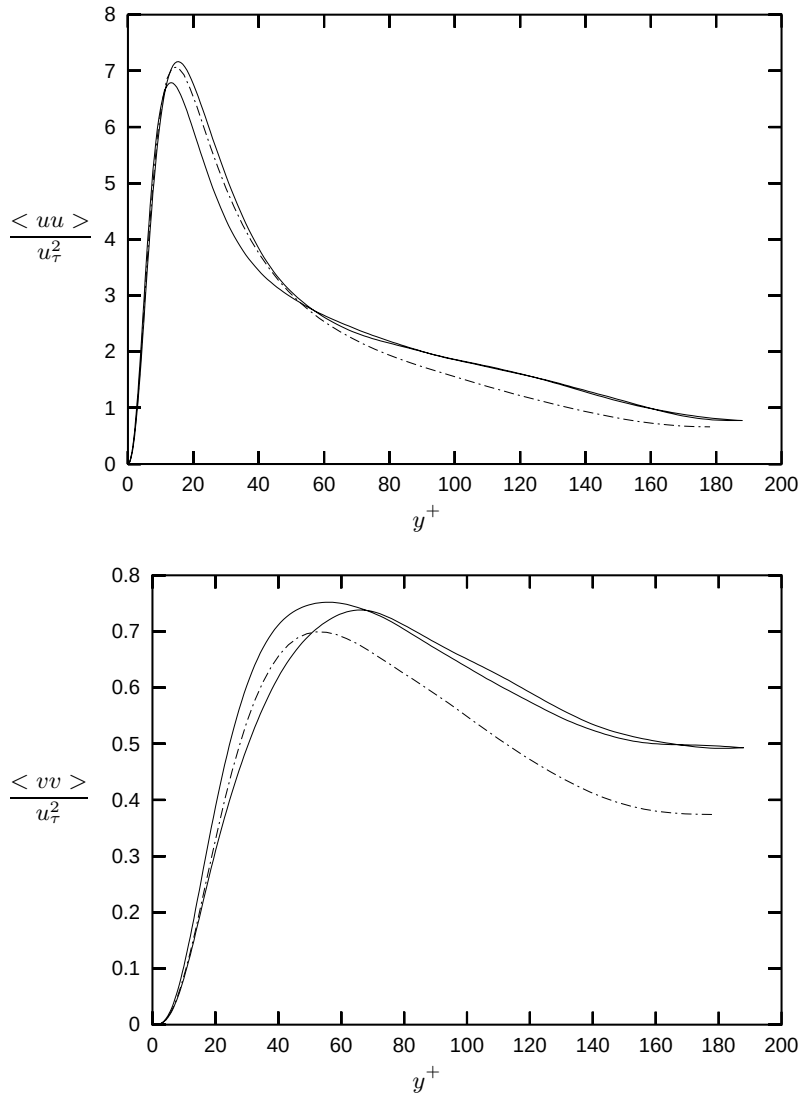

FIGURE 7. Wall-normal profile of various components of the Reynolds stress tensor of the $Re_\tau = 190$ case. Legend as in figure 6.

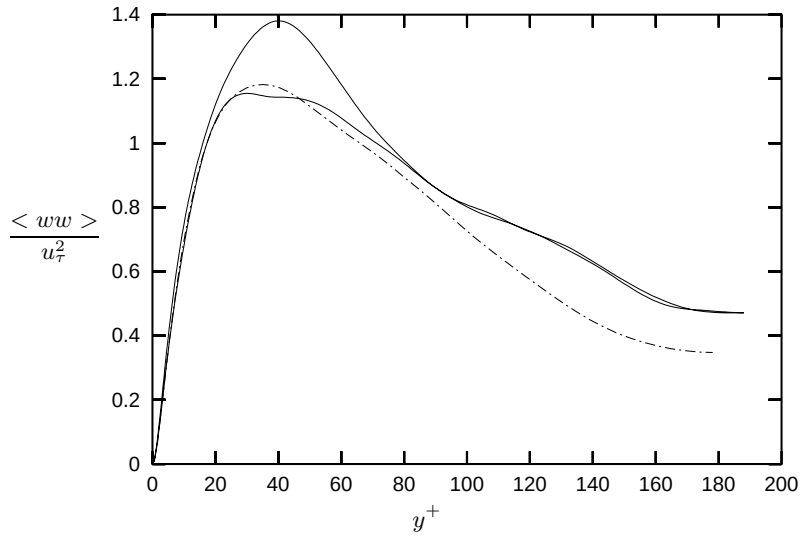

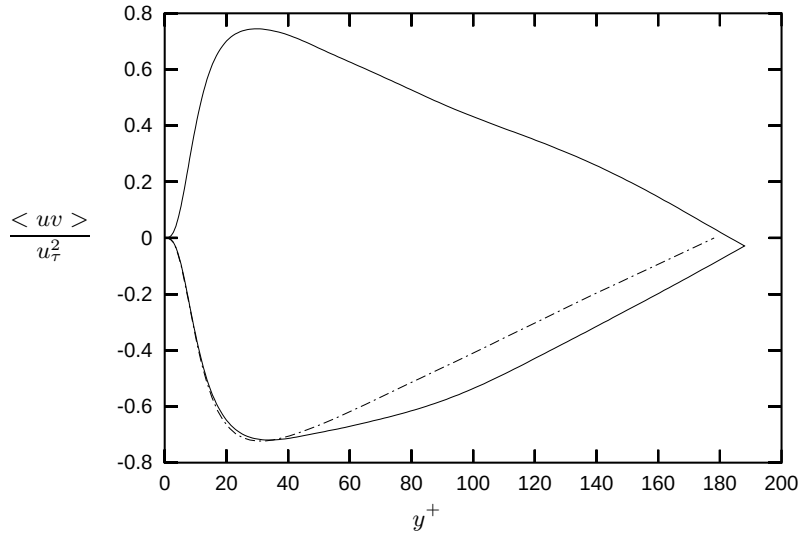

FIGURE 7. *(continued)*

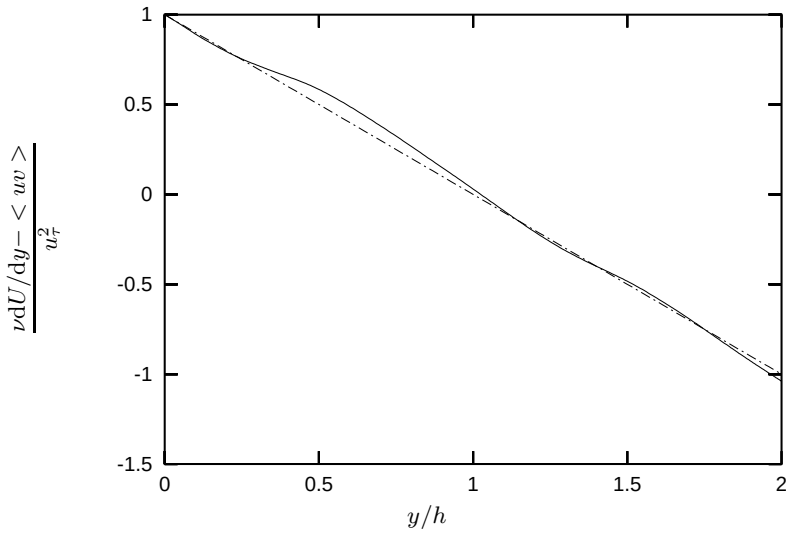

FIGURE 8. Wall-normal profile of the total shear stress of the $Re_\tau = 190$ case. Legend as in figure 6.